AD-A035 025

HIGH STRAIN RATE TESTING OF A LOW CARBON STEEL TO HIGH STRAINS OVER A RANGE OF TEMPERATURES USING A TORSIONAL HOPKINSON-BAR APPARATUS

OXFORD UNIVERSITY (ENGLAND)

SEPTEMBER 1974

UNIVERSITY OF OXFORD

DEPARTMENT OF ENGINEERING SCIENCE

REPORT

ENGINEERING LABORATORY
PARKS ROAD
OXFORD

High Strain Rate Testing of a Low Carbon Steel to High Strains over a Range of Temperatures, Using a Torsional Hopkinson-bar Apparatus.

by

M. G. Stevenson and J. D. Campbell

OUEL Report No. 1098/74
September, 1974

ABSTRACT

A recent version of a torsional Hopkinson-bar apparatus, capable of high strains such as found in metal working, is briefly described. The magnitude of axial forces and bending waves in the system during a test is determined and their effects on measured flow stress shown to be negligible.

Adaptions to the system to permit elevated temperature testing are described. At the specimen ends, the titanium alloy elastic bars are extended by steel tubes to which the specimen may be brazed. The end of each tube glued to a titanium alloy bar has an internal diameter which results in an impedance match at the joint. The internal diameter over the remainder of the tube is tapered to keep the impedance along the tube approximately constant for the temperature gradient occurring in a test at 400°C. A simple electric resistance furnace is used for the heating.

Test results for a low carbon free-machining steel are given, for shear strain rates up to 4330/s and temperatures up to 500°C. In all but one case this material fractured in the dynamic tests before the potential strain was realised, but shear strains of about 1.3 were usually obtained. Because of the large strains, adiabatic heating during the dynamic tests had a substantial effect on the stress-strain curves. The dynamic strain ageing effect was clearly evident from the tests at 400°C and 500°C.

1. INTRODUCTION

To obtain stress-strain data for the analysis of high speed forming processes such as strip rolling, wire drawing, ironing and machining, a materials test should be carried out to large strains in one step.

A temperature rise due to near adiabatic heating will then occur during the test as it does during the process. The material in a process may be subject to even greater temperatures than caused by adiabatic heating because of die friction and pre-heating. A suitable testing apparatus for this purpose should therefore have provision for heating of the specimen.

The torsional version of the Hopkinson-bar apparatus lends itself to tests up to high strains (Ref. 1). Design of such an apparatus capable of shear strains of 5 at shear strain rates of 5000/s has been described in a previous paper. (Ref. 2). Investigations of bending and simple axial stresses occurring in the specimen in this apparatus are described in the present report. The apparatus is also well suited to elevated temperature testing since the strain gauges which are used in the measurement of stress and strain during the test may be placed well away from the heated region. The main problem is the attachment of the specimen to the elastic loading and measuring system, one feasible solution being presented here.

2. APPARATUS

A. Basic System. The set-up for a room temperature test and the corresponding wave diagram is shown in Fig. 1. There are two elastic bars, AC and DE, of titanium 318 alloy (6% Al, 4% V), 25.4 mm in diameter. The specimen is a thin-walled tube with flanges, the nominal dimensions being shown in Fig. 2a. The specimen is located by spigots machined on the ends of the titanium bars (Fig. 2a) and glued to the bars using the epoxy resin adhesive, "Araldite". The input bar AC may be clamped at B while the length AB is pretwisted by hydraulic cylinders acting on the chuck (Ref.3). The clamp design is shown in Fig. 2b. The torque stored in AB may be monitored by strain gauges bonded to it. To store a certain torque, the notched high-tensile bolt shown in Fig. 2b must be sufficiently tight and the bolt torque necessary is found by trial and error and applied by a torque wrench. To release the torque in AB, the bolt is further tightened until it breaks at the notch. This results in a torque T_1, equal to half the stored torque, propagating into the previously unstressed length BC, with a torsional wave speed of 3160 m/s. The rise-time of this torque using the clamp shown in Fig. 2b is approximately 20μs. The specimen dimensions are selected so that it will be plastically strained, and it therefore transmits a lower torque T_2 into the output bar DE. Tinsley Telcon foil torque gauges are bonded to the elastic bars in the positions shown in Fig. 1 to measure T_1 and T_2. A double pair of gauges is placed on opposite sides of the bar in each position and connected in a full bridge circuit to cancel signals due to any bending waves. The gauges are energised by a stabilised

D.C. supply set at 10V. The gauge outputs for T_1 and T_2 are amplified and displayed on a Tektronix 551 dual-beam oscilloscope, triggered by the opening of a circuit caused by the movement of one arm of the clamp. Typical traces are shown on the right of Fig. 1. The torque measuring system is calibrated by dead weights applying a couple at the loading chuck, with a solid dummy specimen glued to the bars and the assembly clamped at E (Fig. 1). Further details of calibration equipment and instrumentation are described by Clyens (Ref. 3).

At any time t, measured from the first rise of a torque trace, T_1 and T_2 may be measured and used to find the specimen strain rate at that time from (Ref. 4) :

$$\dot{\gamma} = \frac{2\left[T_1(t) - T_2(t)\right]}{J\rho c} \cdot \frac{r_m}{\ell} \qquad (1)$$

where J is the polar moment of area of the elastic bars, ρ their density and c the torsional wave speed in them. r_m is the mean radius of the specimen tube and ℓ its gauge length (1.27 mm in Fig. 2a). The specimen strain at time t is found by numerical integration of strain rates found from (1) for time intervals up to t. The corresponding specimen shear stress is found from

$$\tau = \frac{T_2(t)}{2\pi r_m^2 h} \qquad (2)$$

where h is the tube wall thickness.

B. Measurement of Axial Stresses

If equation (2) is to give the shear flow stress of the specimen material at any time, then it is essential that axial stresses throughout the tube wall be absent or negligible. There does not appear to be any feature of the

loading system which could induce a steady axial stress in the system. It is possible, however, that such a stress could occur within the specimen itself at high shear strains. Fluctuating stresses in the axial direction may also occur as a result of bending waves passing along the bar.

The presence of a steady axial stress, i.e. an axial force in the bars during the test, was investigated first. Tinsley Telcon linear foil gauges, type 13/250/E/C, were cemented to the output bar adjacent to the torque gauges in the arrangement shown in Fig. 3. This arrangement was chosen with the aims of cancelling any effect due to bending, and of getting a suitable sensitivity. Since there were two gauges in each arm it was possible to raise the bridge voltage to 18V, which was supplied by dry cells. The sensitivity of this system to axial force was determined directly by setting the output bar vertical and loading it with weights. The result agreed reasonably with calculations based on the bridge circuit characteristics and the elastic modulus of the bar. The output of the axial load bridge during a typical test is shown by the lower trace of the oscilloscope photo in Fig. 3, in which the upper trace gives T_2 . The first deflection of the axial load trace occurs before that of the output torque trace showing that it must be caused by a bending wave which travels faster than the torsional wave. Clearly then, this circuit does not entirely cancel bending effects, possibly because of the length of the bar over which the gauges are spread. After the early fluctuations, however, a relatively steady value results for most of the test time, being interrupted before the end of the test by more fluctuations which appear to be the reflection of the first bending wave from the free end of the output bar.

The average value of the steady part of the trace represents an axial load of approximately 300 N which has a negligible effect on the measured shear flow stress (Appendix 1A).

Bending stresses in the elastic output bar, transmitted by the specimen during a test, were measured using a bridge circuit made up from half of the axial force gauges (Fig. 4). This circuit could be used to measure bending in the vertical or horizontal planes, by rotation of the output bar to an appropriate position before gluing in the specimen. The result of a measurement in the vertical plane during a typical test is shown in Fig. 4. It is shown in Appendix 1B that the peak values of the bending moment oscillations represent a bending moment of approximately 12 Nm, implying a peak direct stress on the specimen of approximately 89 MN/m^2. This direct stress would cause a maximum error of only about 1% in the measured shear flow stress (Appendix 1B). Even without these calculations it is evident from the traces in Fig. 4 that the bending wave has a negligible effect on the output torque since the torque trace remains smooth while the bending trace oscillates, passing through zero several times. Fluctuations were evident in output torque traces for smaller diameter specimens (9.525 mm I.D.), probably because the bending moment caused much greater direct stresses in them. Similar calculations to those described above showed that the measured shear flow stress could be affected by as much as 6%. For this reason results for the smaller specimens were discarded.

Bending was also measured in the horizontal plane by rotating the output bar through 90° and retaining the gauge connections shown in Fig. 4. The resulting bending trace was similar to that found for vertical bending, but of only

half the magnitude. The vertical bending wave therefore appears to be the main problem. In a test where a solid dummy specimen was glued between the bars in place of a tubular specimen, the specimen remained elastic and transmitted a vertical bending wave of maximum amplitude 26 Nm (19 ft. lb.). This was about the same magnitude as the torque required to break the notched bolt, so the present bolt breaking method appears to be responsible for the vertical bending wave. Horizontal bending appears to arise from pre-twisting of the input bar which causes a static bending of this bar which is suddenly released when the torque is released. A more rigid bearing near the clamp should almost eliminate this effect. In the test results given here, the above problems have no significant effect. To achieve higher strain rates, however, stronger clamp bolts would be required, giving larger breaking torques and bending waves. The clamp design would therefore need to be revised.

C. Adaptions for Heated Specimens

To carry out elevated temperature tests with the torsional Hopkinson-bar system, there are two main problems to be overcome, viz. attachment of the specimen to the elastic bars and allowing for the change of elastic modulus G and density ρ in the heated sections of the bars.

Unlike the compression version of the Hopkinson-bar, the torsion system requires the specimen to be bonded to the elastic bars. This is achieved in tests starting at room temperature with an adhesive, usually epoxy resin, acting on surfaces normal to the bar axis. With mechanical joints, there is danger of the introduction of an axial stress or of slight yielding in the joint which could affect

the shape of the input torque pulse. While adhesives have been developed for high temperature work, their maximum temperatures, at which sufficient strength is retained, are still very limited. Gluing different metal specimens to the titanium bars for high temperature tests is also unlikely to prove successful because of differential thermal expansion. To obtain data on a low carbon streel, reported here, this joining method was therefore not pursued.

Since the specimen is joined to the loading and recording bars, heating must take place in situ, giving rise to temperature gradients in the bars. The elastic modulus G and density ρ would then vary along the bar, causing a variation of the impedance $J\rho c$. This can be taken into account in the analysis of the raw data (Ref. 5), or alternatively, the bar diameter may be varied, to vary J and keep $J\rho c$ constant (Ref. 6).

These problems may be solved for tests on a low carbon steel with the arrangement shown in Fig. 5. Two short tubes of plain carbon steel are glued to the elastic bars to become extensions of them. During heating, the ends of the tubes attached to the titanium bars are cooled with a spray of water so that the glued joint remains at room temperature. Since the tubes are of steel, the steel specimens may be brazed to them in a straightforward way. For the present tests, the specimen was brazed to the two tubes using an induction heater, before gluing the resulting assembly into the apparatus. A silver brazing alloy of m.p. 650^{o}C. was used in the form of 0.076 mm thick foil. Washers were cut from the foil, coated with flux, placed on each side of the specimen, and the specimen then located concentric with the tubes using a mandrel. Fig. 6a shows the separate components

and Fig. 6b the assembly ready for brazing. The assembly was located vertically within the induction heater coil using a pair of aligned vee-blocks as shown in Fig. 7. During heating the vee-block upper clamp was loosened slightly to allow the weight of the upper tube to rest on the specimen, ensuring no gaps in the brazed joint. The 4 kW induction heater required application of heat for just under a minute to allow brazing to take place. During heating and cooling, oxygen was kept from the heated part of the assembly by enclosing it in an asbestos box into which there was a continual flow of argon gas. Some oxidation of the specimen flanges still took place, but the specimen tube itself was almost free of oxide, since it had been much cooler than the flanges during the heating process, firstly because the high frequency system heats the surface of the tube closest to the coil and secondly because of the presence of the locating mandrel which was in contact with the internal diameter of the tube and acted as a heat sink. Heating was relatively slow, probably because the magnetic transformation temperature was reached at the surface.

Brazing with copper shims was attempted but a sufficiently high temperature could not be reached with the 4 kW heater. This restricted the maximum temperature of the tests to 500^{o}C. With copper as the brazing metal, tests could be conducted up to at least 800^{o}C. Alternatively, the specimen could be machined integral with a pair of tubes, although the machining operation would be tedious and difficult and a lot of material would be wasted. In the brazing system, the same tubes may be used repeatedly, the specimen being easily removed from them after a test by induction heating.

The tube internal diameter at the glued (cool) end is selected so that the steel tube impedance is matched to that of the titanium bars, i.e.

$$J_s = \frac{J_t \rho_t c_t}{\rho_s c_s} \qquad (3)$$

where the suffixes s and t refer to steel and titanium respectively, and J for a tube is given by

$$J = \frac{\pi}{2} \left(r_o^4 - r_i^4 \right) \qquad (4)$$

where r_o is the outside radius and r_i the inside radius of the tube. With an outside diameter the same as the bars, i.e. 25.40 mm, the inside diameter of the tubes at the glued ends needed to be 20.72 mm.

The possible variation in impedance along the tubes due to a temperature gradient must also be corrected. Considering the hot and cold ends for a test at 400°C, it is required that

$$J_{400} \rho_{400} c_{400} = J_{20} \rho_{20} c_{20}$$

or

$$J_{400} \sqrt{G_{400} \rho_{400}} = J_{20} \sqrt{G_{20} \rho_{20}} \quad .$$

G for steel decreases approximately linearly with temperature, from 82×10^3 MN/m^2 at 20°C to 74×10^3 MN/m^2 at 400°C (Ref. 7). The coefficient of expansion for this steel in this temperature range is 13.9×10^{-6}/°C so the variation of ρ may also be estimated. This gives

$$J_{400} = J_{20} \sqrt{\frac{G_{20}}{G_{400}} \cdot \frac{\rho_{20}}{\rho_{400}}}$$

$$= J_{20} \sqrt{\frac{82}{74} \times 1.0159}$$

$$= 1.061 \; J_{20}$$

Hence, to maintain the same impedance at the hot end in a test at 400°C, as at the room temperature end, J must be increased by 6.1%. Keeping the outside diameter constant, the inside diameter required at the hot end to achieve this increase in J is 20.31 mm. For ease of manufacture, tubes for a test at 400°C were bored with a straight taper from a diameter of 20.72 mm at one end to 20.31 mm at the other. The temperature distribution along such a tube, set up as in Fig. 5, was measured with a series of Chromel-Alumel thermocouples contacting the outside diameter. Fig. 8 shows this distribution and the resulting variation of J_{pc} for the tapered tubes. This shows J_{pc} to be constant within 0.5%. If the tube bores had not been tapered, the temperature variation would have caused a maximum variation in J_{pc} of 5.7% (Appendix II).

The specimen was heated with an electrical tube furnace made by Wild Barfield Ltd. for use with the Hounsfield Tensometer testing machine. The temperature was measured at the specimen flange using a Chromel-Alumel thermocouple as shown in Fig. 9. The thin copper rings at the cool ends of the tubes in Fig. 9 were used to ensure that the cooling water drained into a tube below the spray and did not flow along the tube. The bars on either side of the elastic bar assembly in Fig. 9 are simply to support the furnace which could easily be slid out of the way when attaching the specimen and tube assembly. Fig. 10 shows the furnace and cooling system in position ready for a test. A rough control on temperature was achieved with the Ether controller shown in Fig. 10 and a thermocouple near the specimen, but as a steady test temperature was reached, the Comark Thermocouple Indicator was used with a thermocouple as in Fig. 9 to

3. EXPERIMENTAL RESULTS

The material tested was a low carbon free-machining steel of composition 0.125%C, 1.15% Mn, 0.37% S, supplied as hot-rolled 64 mm square bar. Photomicrographs of the structure are given in Fig. 11.

A. Tests Starting at Room Temperature

All room temperature tests were performed without the steel tube extensions, i.e. with the bar arrangement in Fig.1 .

i) "Static" Testing at a very low speed was carried out with a typical specimen (Fig. 2), glued in place as usual. The input bar was clamped and the output bar rotated at its normally free end by an electric motor driving through a reduction gearbox. The speed used was 1.03×10^{-3} rad/s. The bar torque was recorded on the oscilloscope whose sweep rate was set to a nominal rate of 10 s/cm , the actual rate being measured with a stop-watch. The strain for any torque reading was calculated from the rotation speed and the sweep rate, a correction being made for the wind-up of the elastic bars (Appendix III). The traces for one of the tests are shown in Fig. 12, while stress-strain points for two static tests are plotted in Fig. 13.

ii) "Dynamic" Oscilloscope traces for two dynamic tests are shown in Fig. 14. In the test giving Fig. 14a, the shear strain rate averaged 2230/s and for 14b, 4330/s. Apart from the initial rise time of approximately 20 μs, the strain rates varied by only ± 5% from the mean values.

The stress-strain curves for these two tests are plotted in Fig.13.

Assuming an adiabatic process, the temperature rise at any strain γ in the dynamic tests is given by

$$\Delta T = \frac{\int_0^{\gamma} \tau \, d\gamma}{\rho \bar{s}} \qquad (5)$$

where $\bar{s}$ is the mean specific heat during the test. At a temperature T ^{o}C, the specific heat of the steel is (Ref.7):

$$s = 420 + 0.504\ T \quad \text{J/kg K.} \qquad (6)$$

A computer program was written to evaluate the shear stress, strain and strain rate, and the temperature, at intervals of 20 or 40 microseconds. To obtain approximate values of ΔT, $\bar{s}$ at a given time was taken to be given by equation (6), using the last calculated temperature. This procedure underestimates ΔT by 5-10%, but a similar error of opposite sign is expected from the neglect of the stored energy of plastic deformation. At a shear strain of unity, the calculated temperature rises were 116 and 119 ^{o}C at strain rates of 2230 and 4330/s respectively; these substantial rises indicate a significant reduction in the work-hardening rate at large strains.

The available test duration, about 1 ms, gave potential shear strains of 2.23 and 4.33 at the two strain rates used. In fact the specimens fractured at strains of about 1.4 and 1.3 respectively. The relatively low ductility of the material is attributed to the presence of manganese sulphide inclusions. These inclusions provide ideal sources for cracks which propagate readily in the absence of a compressive hydrostatic stress.

B. Elevated Temperature Tests

Tests were carried out at starting temperatures of 200°C, 400°C (two tests) and 500°C, and the oscilloscope traces are given in Fig. 15. In all these tests, the steel tube extensions were used, taper bored specifically for the 400°C test. The torque traces for T_1 in all cases show a slight reflection from the joint between the solid input bar and the tube. The torque rises by about 3% at this joint showing that J for the steel tubes is too large and the internal diameter should be increased accordingly for future tests. (To decrease J for the tubes by 3%, the internal diameter at the joint should be increased from 20.72 mm to 20.91 mm, a change in wall thickness of .095 mm.) In the two tests at 400°C, T_1 remains constant as it traverses the tube, while in the test at 200°C it rises slightly and in the test at 500°C it falls slightly. This is consistent with the fact that the taper is matched to a maximum temperature of 400°C. Ideally, different tubes should be made for each test temperature, but in the present tests the temperature range is not very great and the accuracy has not been significantly affected.

Stress-strain curves for the hot tests are given in Fig. 16, together with a curve from one of the room temperature tests. There is little variation in strain rate between the tests of Fig. 16, so the effect of starting temperature may easily be seen. In all the dynamic tests, temperature rises are substantial, and these rises will be less where the stress levels are less. It is therefore useful to plot stress for several different strain levels against actual temperature, i.e. the starting temperature plus the temperature rise. This has been done in Fig. 17 for the tests

represented in Fig. 16, after calculating temperature rises as before.

The increase of flow stress with temperature between 400°C and 500°C, which is evident in Fig. 17, shows that dynamic strain ageing still takes place at a shear strain rate of about 2000/s. This characteristic explains the apparent increase in strain hardening as starting temperature is raised. The adiabatic temperature rise in the room temperature tests tends to soften the material, whereas in a test starting at 400°C, further increases in temperature due to adiabatic heating cause dynamic strain ageing and an increase in flow stress.

In all the elevated temperature tests, the specimen was found fractured after the tests, but in the case of the test starting at 200°C, the potential strain was apparently realised. The specimen in this test may have fractured during reversed straining caused by subsequent wave motion in the elastic bars. Thus, ductility was enhanced by pre-heating to 200°C. Ductility decreased on heating to higher temperatures, however, the 500°C specimen breaking at a strain of only 0.82.

Repeatability for this testing system was not thoroughly examined, but some indication is gained from the two tests at 400°C. Here, the average difference between the tests was approximately 3%. A repetition test was also made at room temperature when using specimens of 9.525 mm inside diameter, with a similar result.

4. CONCLUSIONS

The torsional Hopkinson-bar system has been shown to give valid results for high strains and elevated temperatures. The clamp design needs to be improved for tests at strain rates greater than 5000/s and copper brazing will be required for temperatures greater than 500^{o}C.

The results presented for a low carbon free-machining steel show a substantial effect of adiabatic heating. At lower starting temperatures, this effect reduces apparent strain hardening to zero and even negative rates, while at high temperatures it enhances it. More tests are required to check on accuracy and it would be particularly interesting to examine further the effect of starting temperature on ductility. Tests on more ductile materials will allow the system's full potential for large strain to be realised.

ACKNOWLEDGEMENTS

The authors would like to thank Dr. A. Eleiche, who made up the thermocouples, Dr. B. Dodd for assistance with computer programming, Mr. R. Sawala for the photomicrographs, and the workshop staff of the Dept. of Engineering Science for their prompt service and good workmanship.

The first author is grateful for financial assistance from the British Council and the Study Leave Assistance Fund of the University of New South Wales during the period when the experimental work was carried out. Financial support for the work has also been provided by the Air Force Materials Laboratory (LLN), United States Air Force under Grant AFOSR 71-2056.

REFERENCES

1. CAMPBELL, J.D., 1973 Matls. Sci. and Engg., 12, 3.

2. STEVENSON, M.G., 1974 Proc. Conf. on Mech. Props. of Matls. at High Rates of Strain, Paper 29, The Inst. of Physics, London.

3. CLYENS, S., 1973 M.Sc. Thesis, Dept. Engg. Sci., Oxford University.

4. TSAO, M.C.C. and CAMPBELL, J.D., 1973 Rept. No. 1055, Dept. Engg. Sci., Oxford University.

5. CHIDDISTER, J.L. and MALVERN, L.E., 1963 Exp. Mechs., 3, 81.

6. ELEICHE, A. and DUFFY, J., Private communication.

7. NATIONAL PHYSICAL LABORATORY, The Physical Properties of a Series of Steels, Part II, The Iron and Steel Institute, London, 1946. (Quoted in METALS HANDBOOK, American Society for Metals, Cleveland, Ohio, 1948, p.313).

APPENDIX 1A

Effect of Axial Load on Measured Shear Stress

For the measured axial load of 300 N , the axial stress in a specimen of 0.50 mm wall thickness is

$$\sigma_x = \frac{300 \times 10^4}{\pi(.84375^2 - .79375^2)}$$

$$= 11.66 \text{ MN/m}^2$$

In a typical dynamic test, the measured shear stress is 350 MN/m^2 . The state of stress in the tube wall may then be described by $\sigma_x = 11.66$ MN/m^2 , $\sigma_y = 0$ and $\tau_{xy} = 350$ MN/m^2 . The maximum shear flow stress is then given by

$$k = \sqrt{\tau_{xy}^2 + \left(\frac{\sigma_x}{2}\right)^2} \qquad (1A)$$

$$= 350.05 \text{ MN/m}^2$$

Using von Mises' yield criterion instead of Tresca's the effective shear flow stress is given by

$$k = \sqrt{\tau_{xy}^2 + \frac{\sigma_x^2}{3}} \qquad (1B)$$

$$= 350.06 \text{ MN/m}^2.$$

Thus the measured shear stress underestimates the shear flow stress by less than 0.02%.

APPENDIX 1B

Bending Moment Calculations

For the circuit in Fig. 4, the output voltage is given by

$$V_o = \frac{F\ V_i}{4} (-\varepsilon_5 + \varepsilon_6 - \varepsilon_2 + \varepsilon_1) \qquad (2A)$$

where F is the gauge factor of the strain gauges used, V_i is the input voltage and ε_1, ε_2, ε_5 and ε_6 are the strains in the respective arms. Considering the gauges in the position shown in Fig. 3 and bending in the vertical plane, (1A) becomes

$$V_o = \frac{F\ V_i}{4} \times 2.6\ \varepsilon_b$$

where ε_b is the maximum bending strain at the upper surface, whence

$$V_o = \frac{2.1 \times 10}{4} \times 2.6\ \varepsilon_b$$

and

$$\varepsilon_b = \frac{4\ V_o}{2.1 \times 10 \times 2.6} = .07326\ V_o$$

From bending trace in Fig. 4, the maximum absolute value of V_o is 0.95 mV

Hence $\varepsilon_b = .07326 \times 0.95 \times 10^{-3}$

$= .0696 \times 10^{-3}$

The corresponding maximum bending stress is then

$$\sigma_b = E\ \varepsilon_b$$

where E is the elastic modulus for the titanium alloy, hence

$\sigma_b = 106.2 \times 10^3 \times .0696 \times 10^{-3}$ MN/m^2

$= 7.39$ MN/m^2.

The moment causing this stress on the titanium alloy bar surface may be calculated from :

$$M = \sigma_b \frac{\pi r^3}{4},$$

where r is the bar radius. This gives

$$M = \frac{7.39 \times 10^6 \times \pi}{4} \times \frac{2.54^3}{8} \times 10^{-6}$$

$$= 11.889 \text{ Nm}.$$

To simplify the stress distribution in the specimen due to this bending, it is assumed that the specimen is rigid - perfectly plastic and the stress is therefore uniformly distributed on each side of the neutral axis, but changes sign at the neutral axis.
The magnitude of the uniform stress is then given by

$$\sigma_x = \frac{M}{4hr_m^2} . \qquad (3A)$$

For the results described here, most specimens had a wall thickness, h , of approximately 0.50 mm, while all had an internal diameter of 15.88 mm , giving a mean radius, r_m , of 8.19 mm. Hence, from equation (3A),

$$\sigma_x = 88.62 \text{ MN/m}^2 .$$

Taking the measured shear stress, τ_{xy}, as 350 MN/m^2, the flow stress in pure shear, given by equation (1A) or (1B), is 352.8 or 353.7 MN/m^2 respectively. The measured value thus underestimates the flow stress by at most 1.06% .

APPENDIX II

Variation of $J \rho c$ in Heated Section of System

Distance from centre, cm	Temp. $^{o}C.$	Inside radius, r_i mm	J m^4 x 10^{-8}	ρ kg/m^3 x 10^3	G N/m^2 x 10^9	$J\sqrt{\rho G}$ (Variable J) kgm^2/s x 10^{-2}	$J_{20}\sqrt{\rho G}$ (Constant J) kgm^2/s x 10^{-2}
0	400	10.155	2.4159	7.739	74	57.81	54.49
3	350	10.203	2.3841	7.755	75	57.50	54.91
6	250	10.252	2.3511	7.787	77	57.57	55.75
9	145	10.300	2.3184	7.821	79	57.63	56.60
12.7	20	10.360	2.2768	7.862	82	57.81	57.81

APPENDIX III

Corrections for Wind-up of Elastic Bars in Static Torsion Test.

Total twist of the elastic system for a torque T is given by:

$$\theta = \frac{TL}{JG}$$

$$= \frac{2L}{\pi r^4 G} \cdot T$$

Where r = the bar radius = 1.27×10^{-2} m

L = the bar length between the drive end and the clamp = 2.25 m

G = shear modulus of the bars

= 44.816×10^9 N/m^2 ,

giving

$$\theta = 1.2286 \times 10^{-3} T \text{ radians.}$$

For Test of Fig. 12:

T is measured at 2 cm intervals from the initial yield point, which is detected by a kink in the torque trace. Sweep rate = 9.4 s/cm and Output shaft speed is 1.03×10^{-3} rad./s , so 2 cm interval represents:

$2 \times 9.4 \times 1.03 \times 10^{-3}$ rad.

= 19.36×10^{-3} rad.

Other data: Torque trace : 1 mm = 2.55912 Nm

Mean spec. radius, r_m = 8.1955 mm

Wall thickness, h = 0.516 mm

Gauge length, ℓ = 1.27 mm

(See over for calculations)

Static Test, Stress-Strain Calculations

Position cm	T mm	τ Mn/m^2	θ Total, measured from y.p. 10^{-3} rad.	θ due to bar wind-up, 10^{-3} rad.		θ at specimen 10^{-3} rad	$\gamma \left(\theta_{spec} \times \frac{r_m}{l}\right)$
				Total	Measured from y.p.		
0 (y.p.)	12.2	143.4	0	38.36	0	0	0
2	15.5	182.2	19.36	48.73	10.37	8.99	0.058
4	18.2	213.9	38.73	57.22	18.86	19.87	.128
6	21.5	252.7	58.09	67.60	29.24	28.85	.186
8	23.5	276.2	77.46	73.89	35.53	41.93	.271
10	24.7	290.3	96.82	77.66	39.30	57.52	.371
12	25.8	303.2	116.18	81.12	42.76	73.42	.474
14	26.7	313.8	135.55	83.95	45.59	89.96	.581
16	28.0	329.1	154.91	88.04	49.68	105.23	.679
18	28.5	334.9	174.28	89.61	51.25	123.03	.794
20	29.0	340.8	193.64	91.18	52.82	140.82	.909
22	29.5	346.7	213.00	92.75	54.39	158.61	1.024
24	29.7	349.0	232.37	93.38	55.02	177.35	1.144
26	30.5	358.4	251.73	95.90	57.54	194.19	1.253
28	30.5	358.4	271.10	95.90	57.54	213.56	1.378
30	30.7	360.8	290.46	96.52	58.16	232.30	1.499
32	31.0	364.3	309.82	97.47	59.11	250.71	1.618
34	31.0	364.3	329.19	97.47	59.11	270.08	1.743

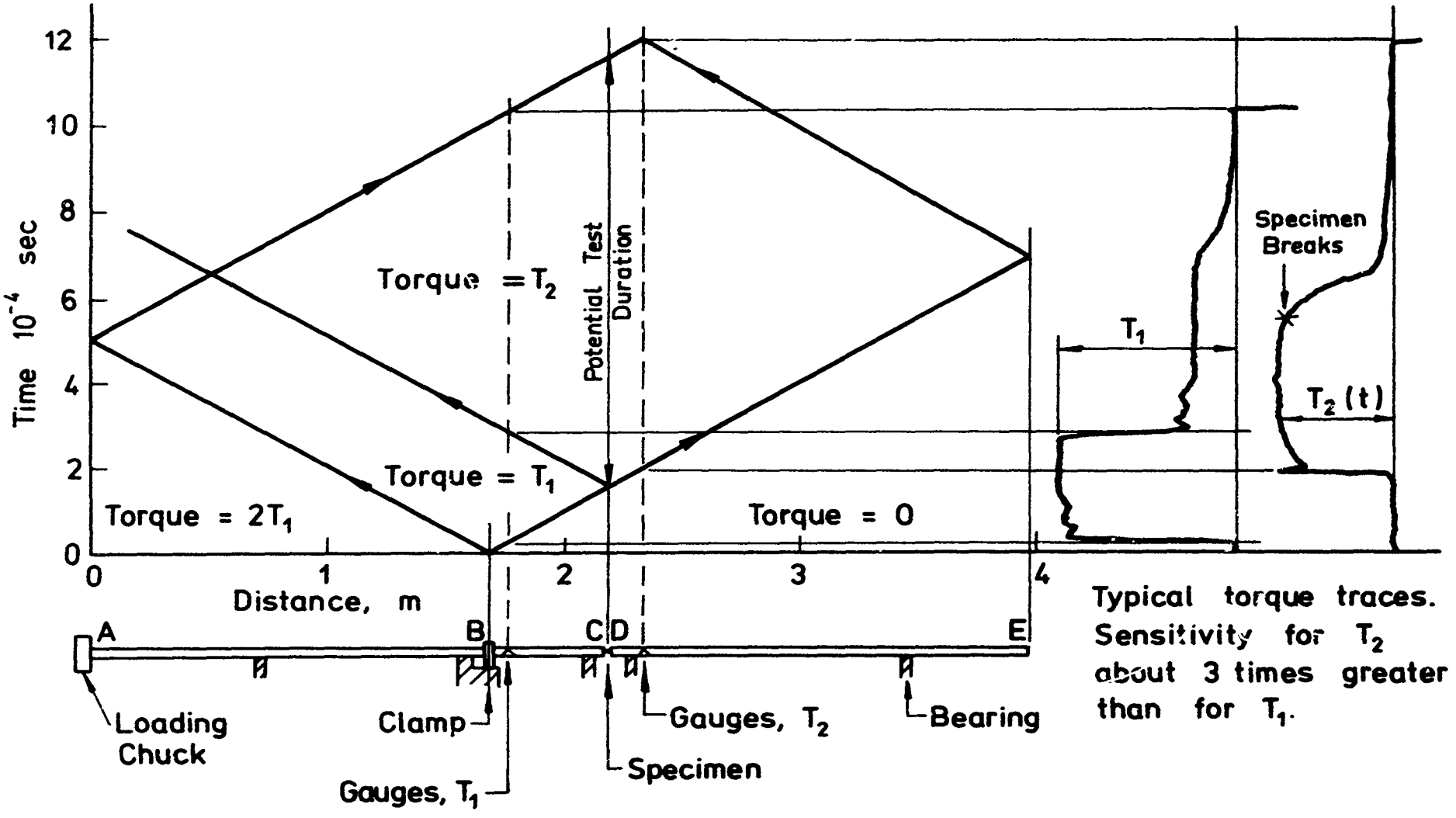

Fig. 1 Set-up and wave diagram for tests starting at room temperature.

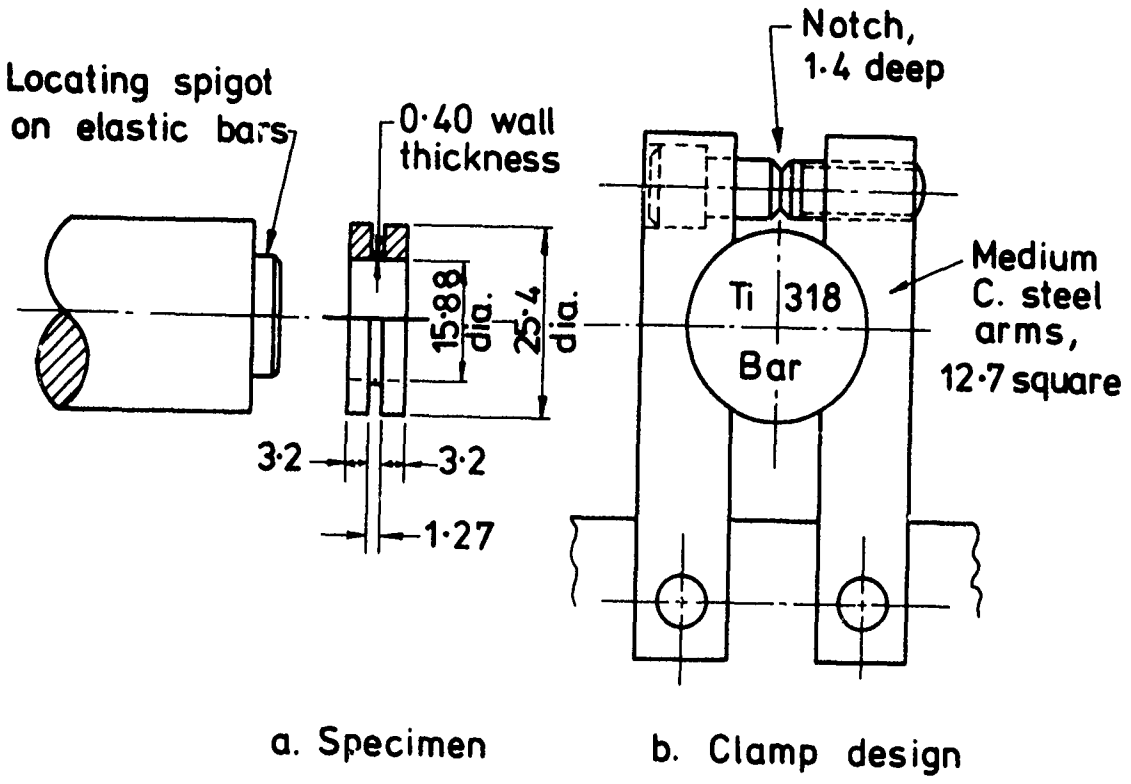

Fig. 2 Specimen and clamp designs - all dimensions in mm.

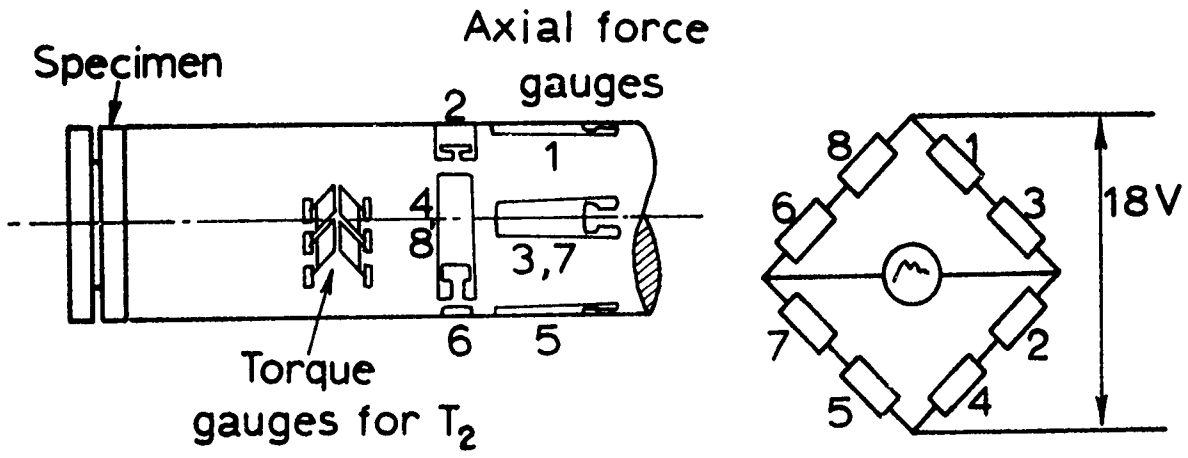

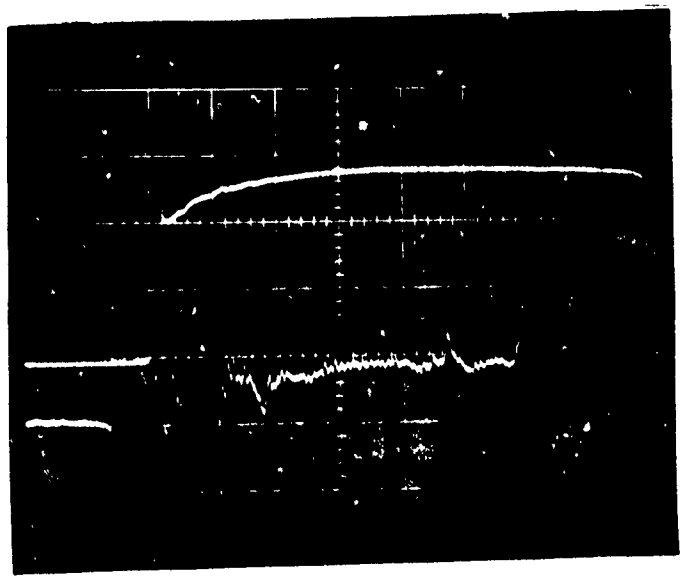

Fig. 3 Arrangement and connection of axial force strain gauges, and corresponding oscilloscope trace. Settings: upper beam (T_2) - 2 mV/cm, lower beam (axial force) - 0.2 mV/cm, sweep rate - 100 μs/cm.

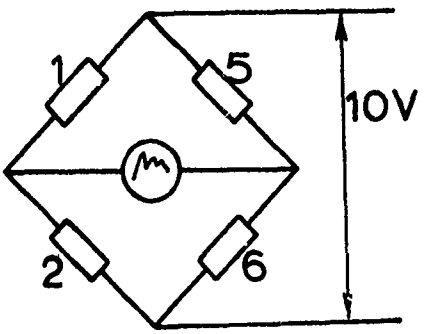

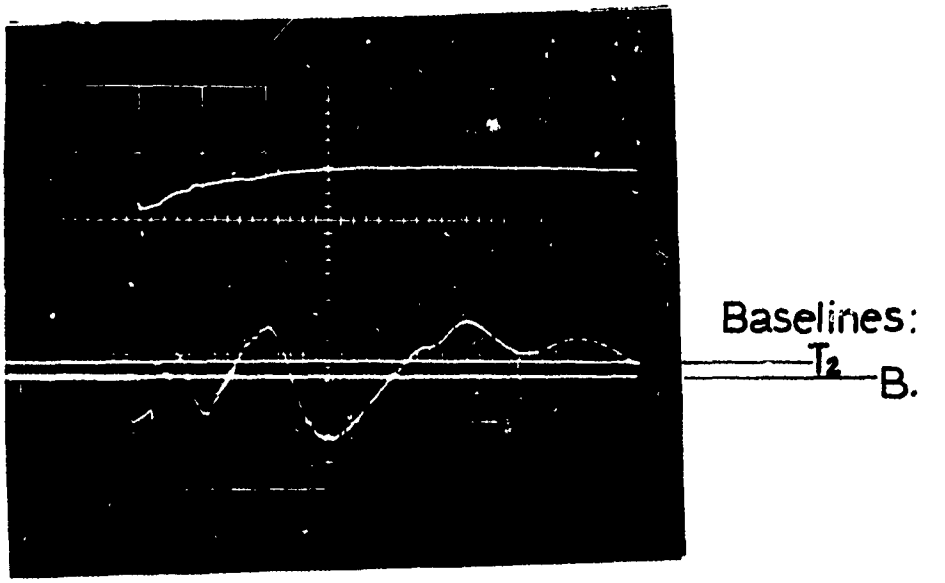

Fig. 4 Connection of gauges shown in Fig. 3 to measure bending in the vertical plane and corresponding oscilloscope trace, including baselines. Settings: upper beam (T_2) - 2 mV/cm, lower beam (bending) - 1 mV/cm, sweep rate - 100 μs/cm.

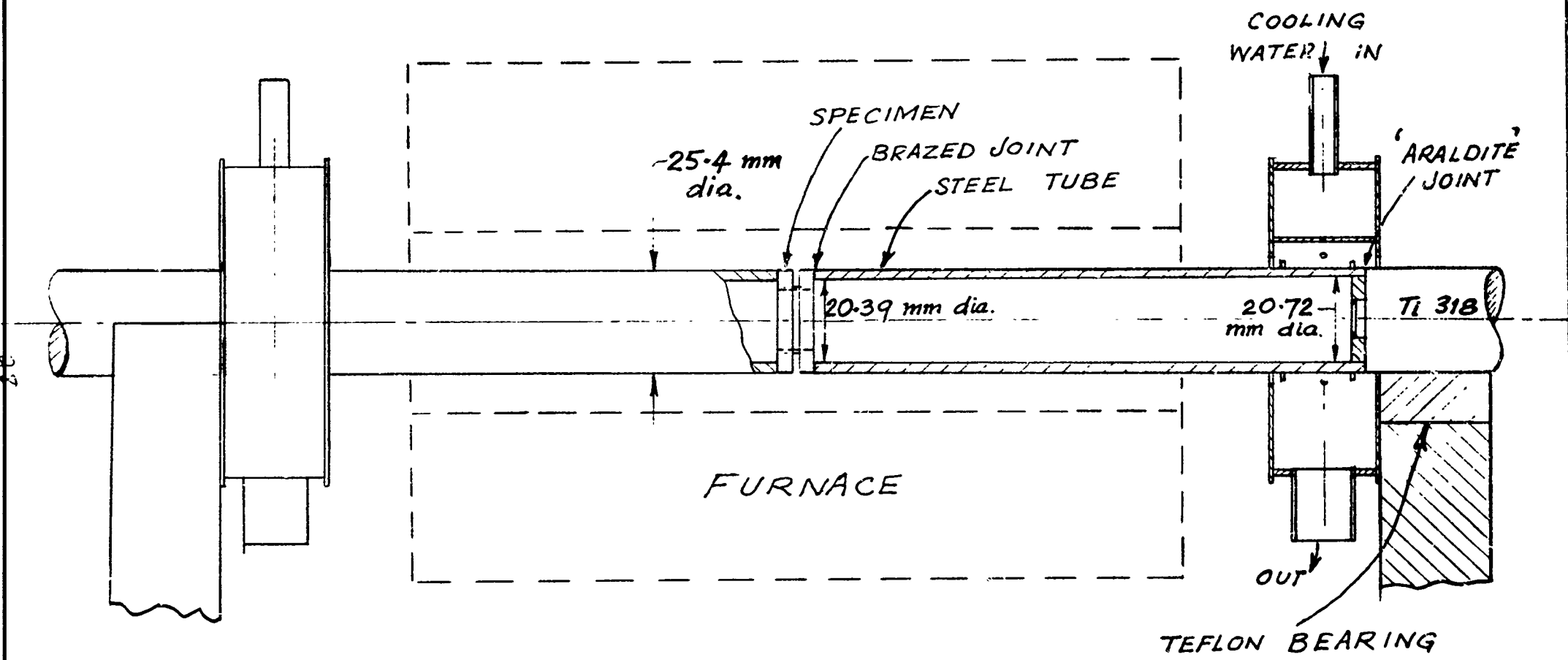

Fig. 5. Elastic bar extensions in heated section of system.

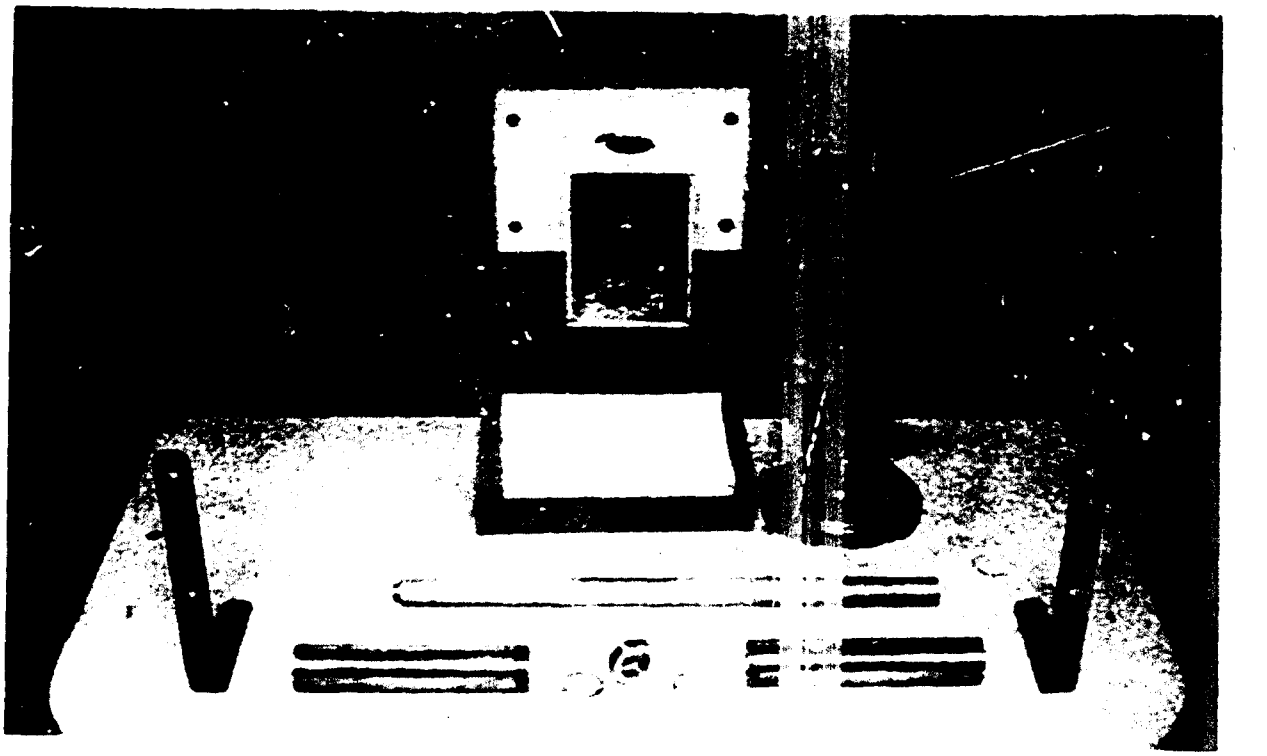

a.

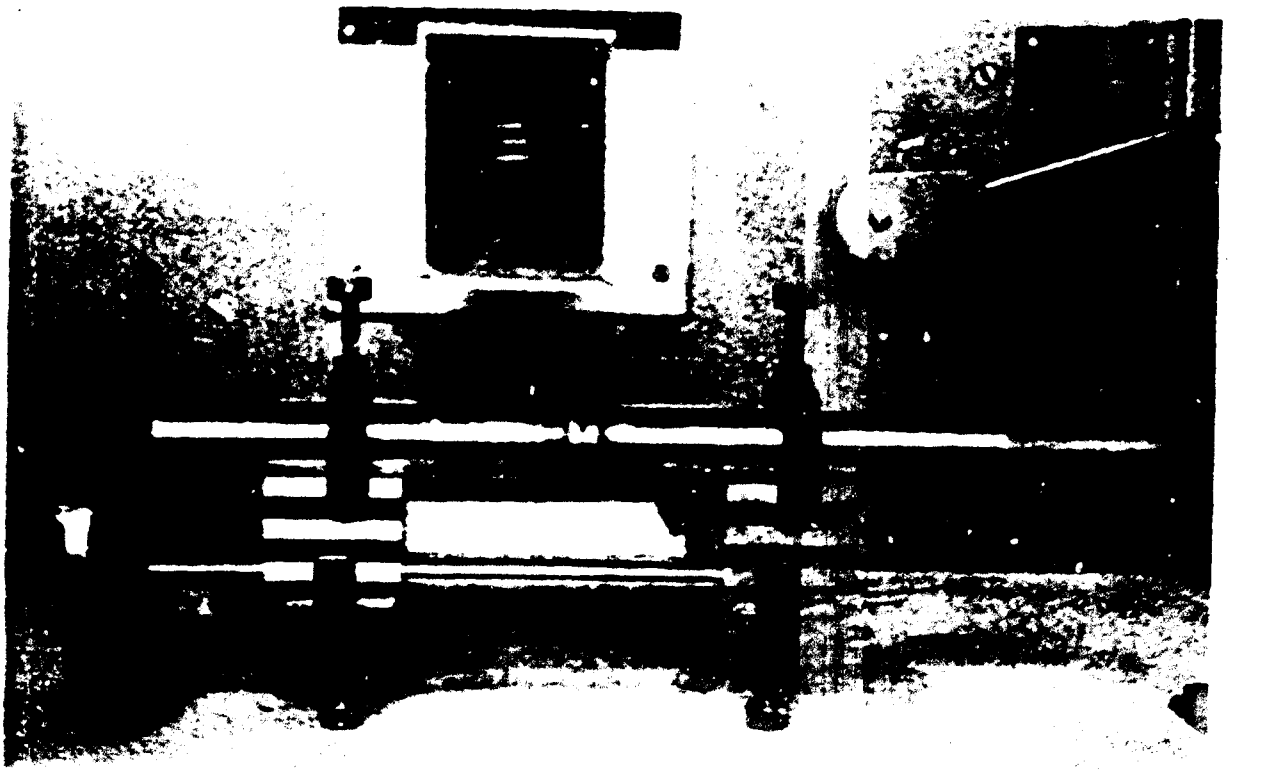

b.

Fig. 6 Brazing of specimen to steel tube a) separate components b) components assembled.

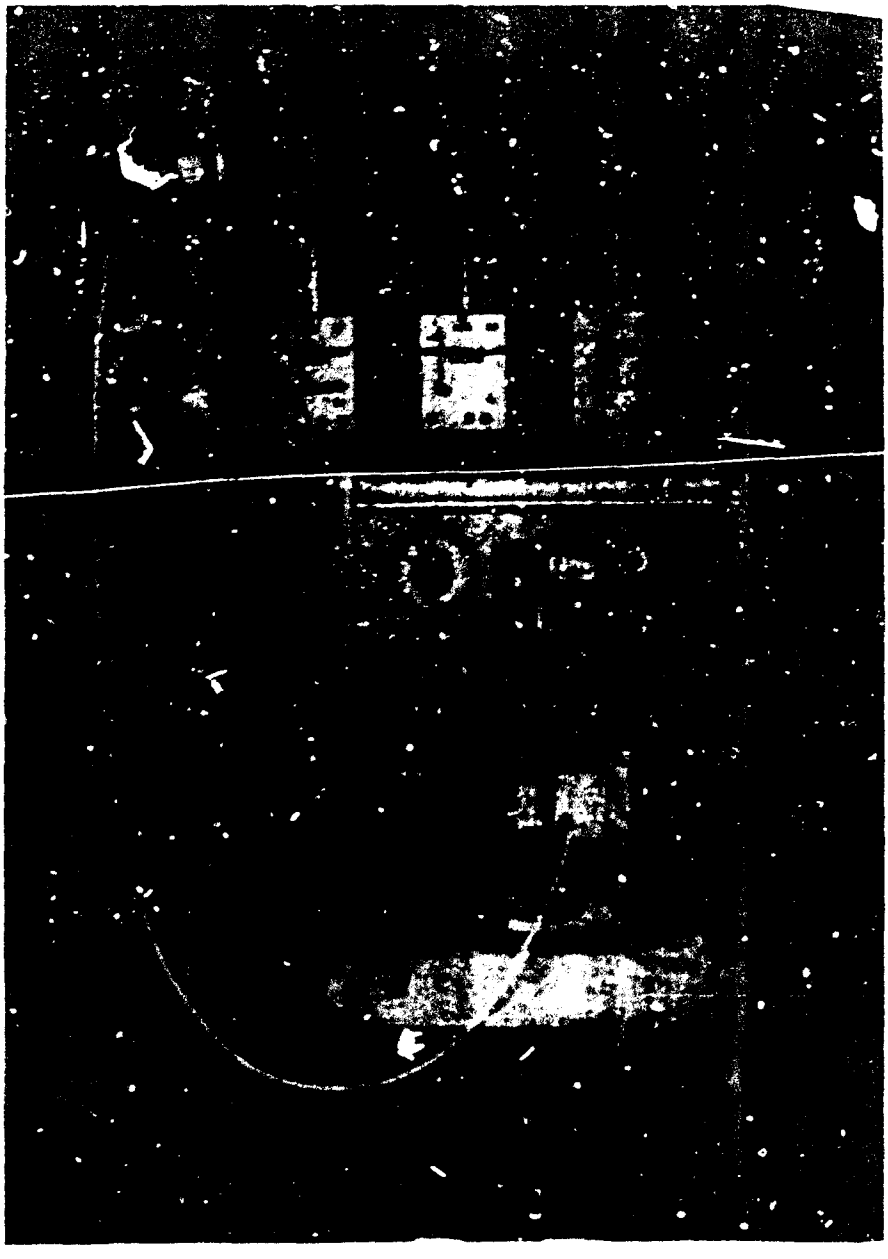

Fig. 7 Tube and specimen assembly located in induction coil for brazing.

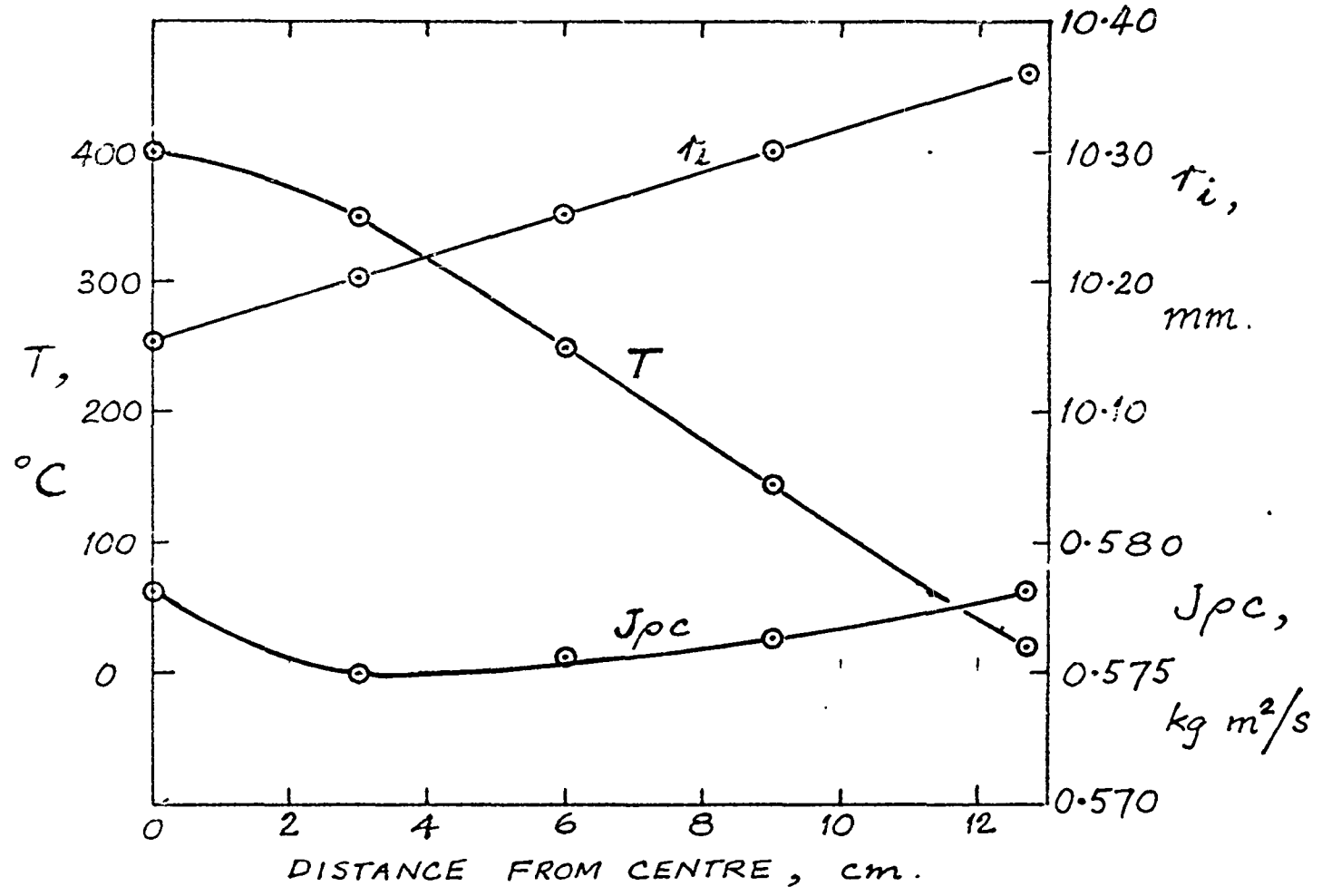

Fig. 8 Variation of temperature, T, internal radius, r_i, and impedance, Jpc, along steel tubes for test temperature of 400 °C.

Fig. 9 Specimen and tube assembly in place, showing thermocouple which will be slid on to specimen flange.

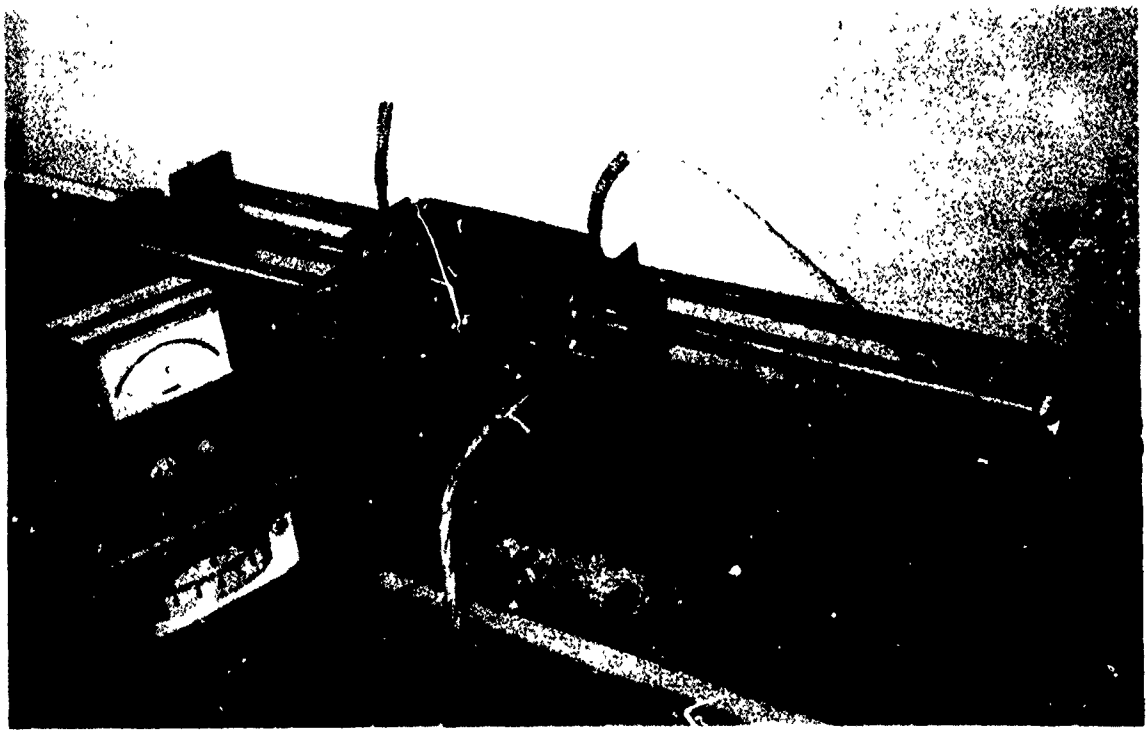

Fig. 10 Furnace and cooling system in position for a test.

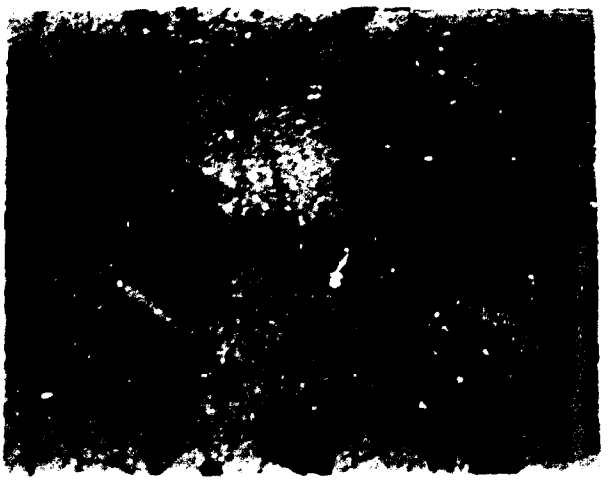

a.

b.

Fig. 11 Specimen material microstructure a) x 300 , b) x 1000.

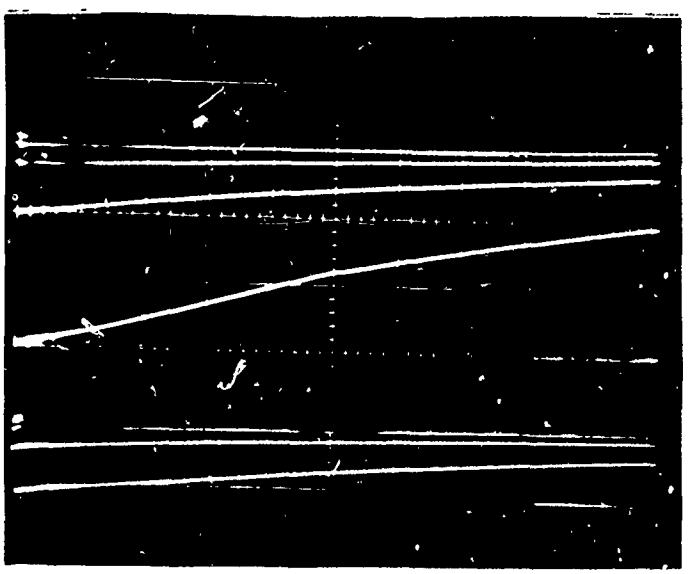

Fig. 12 Oscilloscope traces for static test. Upper traces used where 1 mm = 2.559 Nm. Sweep rate = 9.4 s/cm.

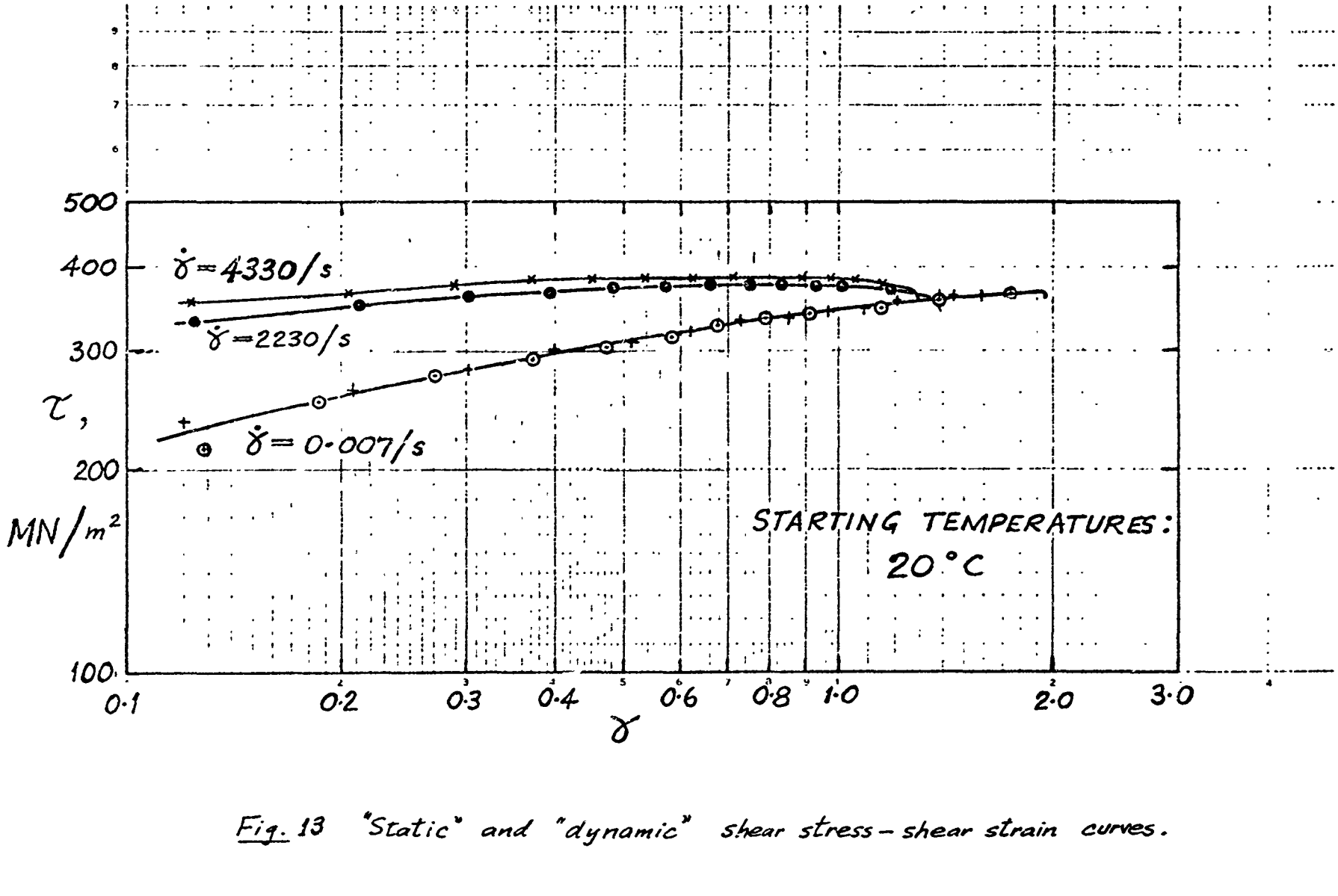

Fig. 13 "Static" and "dynamic" shear stress – shear strain curves.

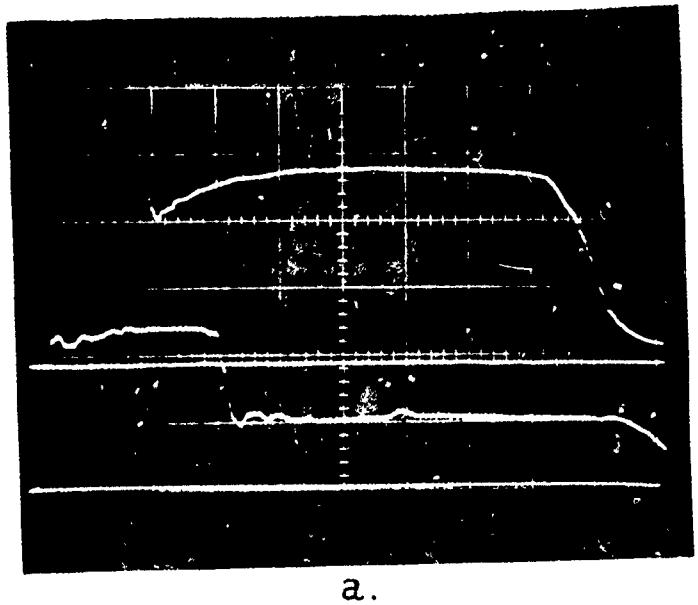

a.

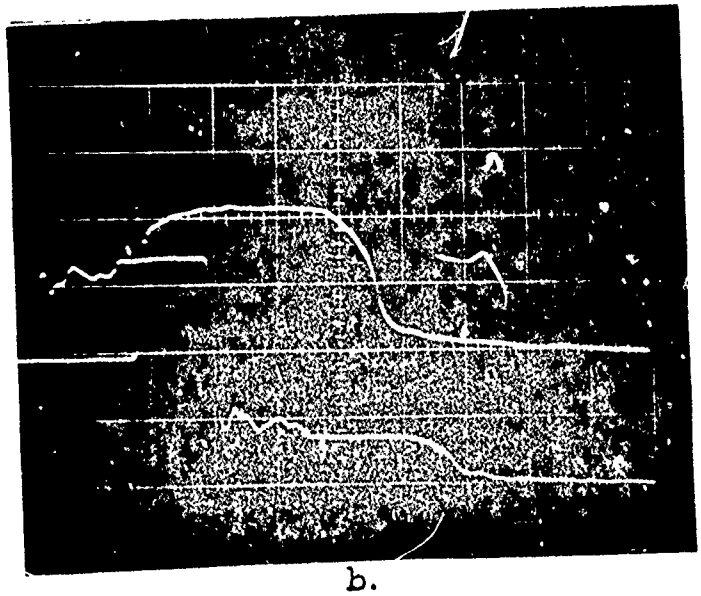

b.

Fig. 14 Oscilloscope traces for dynamic tests at room temperature. Settings the same for a) and b), viz.

T_1 (lower trace) - 75.46 Nm/cm,

T_2 (upper trace) - 28.43 Nm/cm, Sweep rate - 100 μs/cm.

Wall thicknesses: a) 0.52 mm

b) 0.40 mm

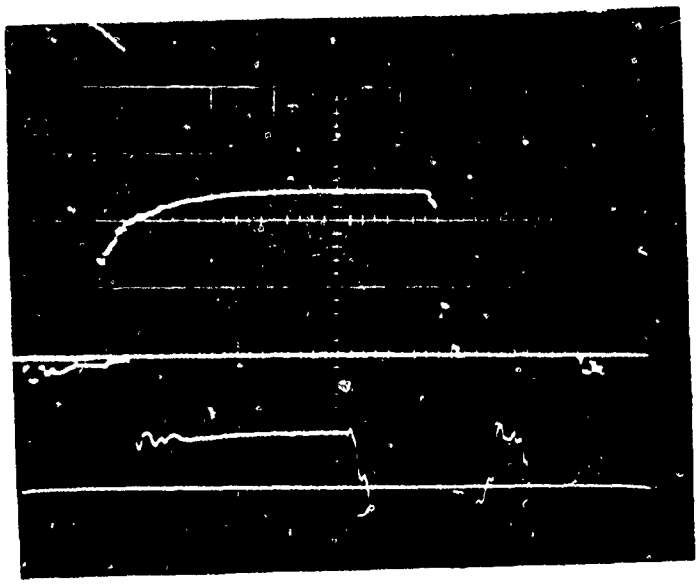

a.

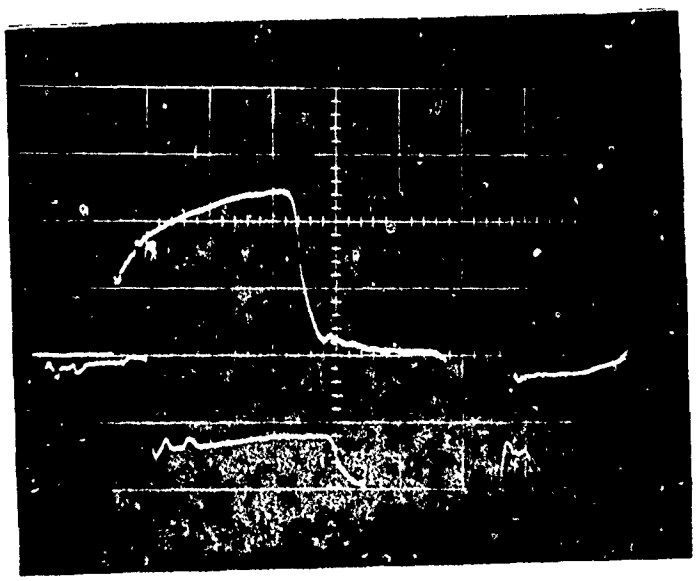

b.

Fig. 15 Oscilloscope traces for elevated temperature testing, a) 200°C , b) 400°C , c) 400°C and d) 500°C.

Settings for all traces:

T_1 (lower traces) - 75.46 Nm/cm

T_2 (upper traces) - 28.43 Nm/cm

Sweep rate - 200 μs/cm.

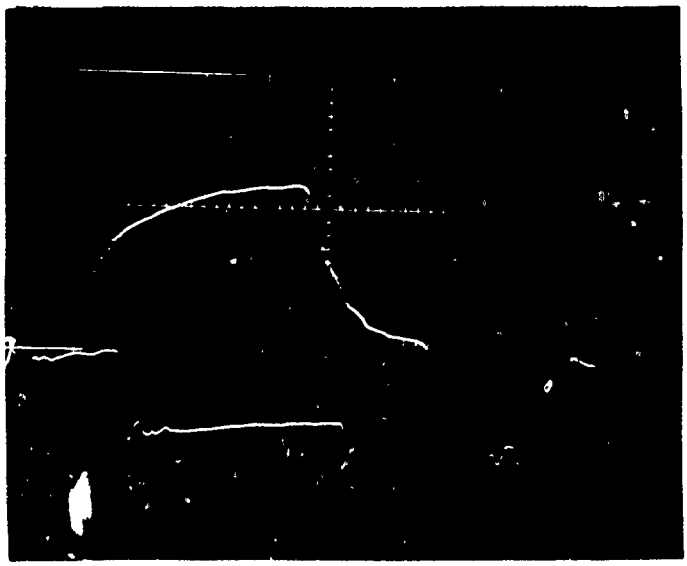

c.

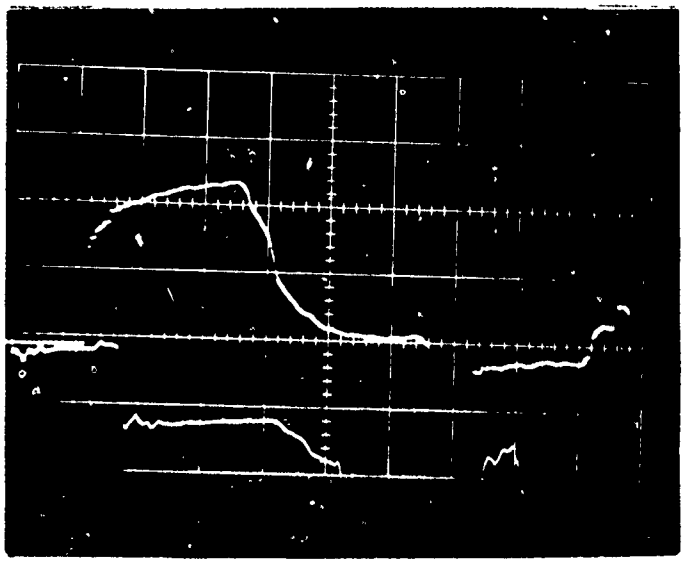

d.

Fig. 15 (contd.)

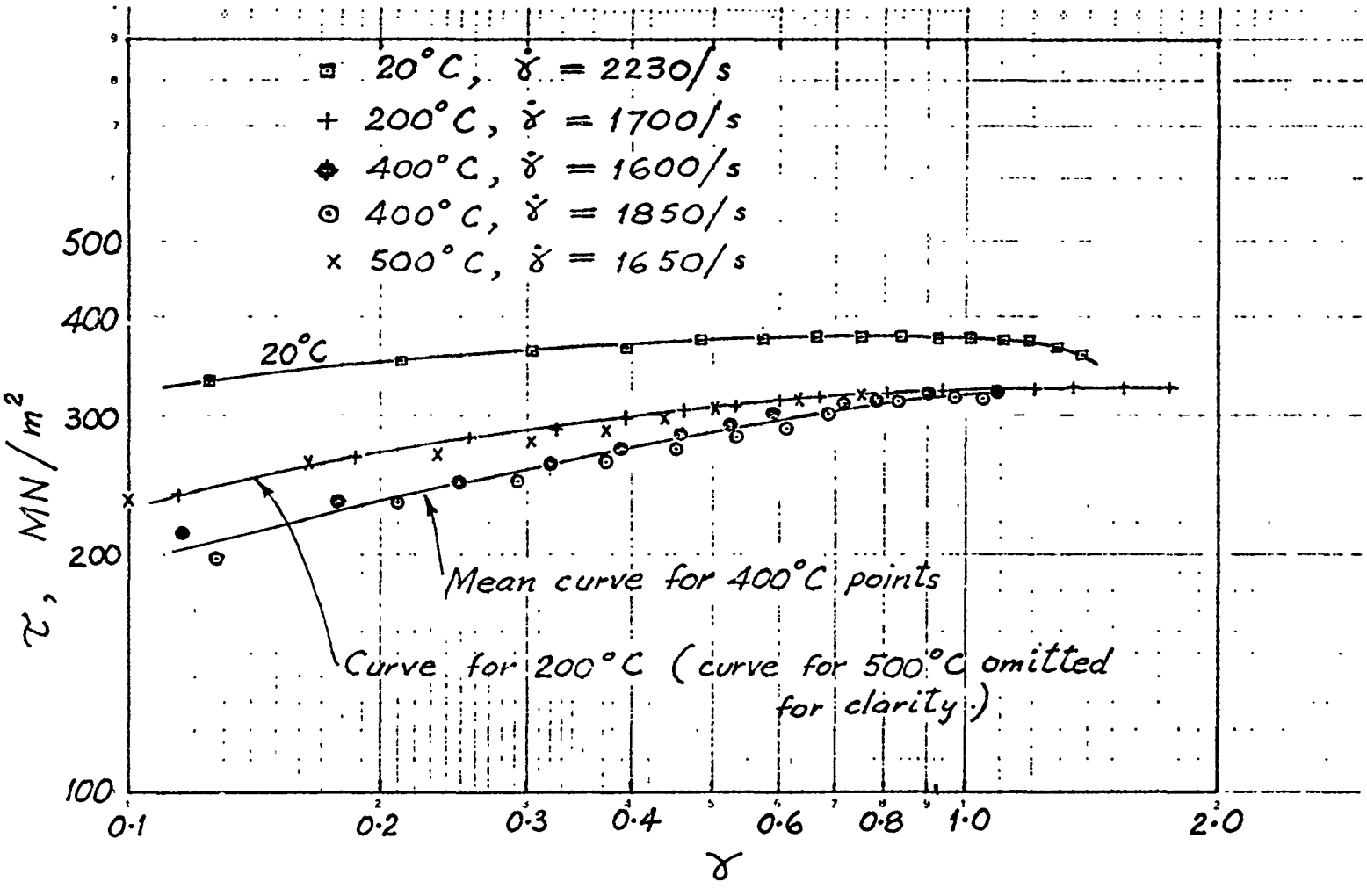

Fig. 16. Shear stress–shear strain curves for different starting temperatures.

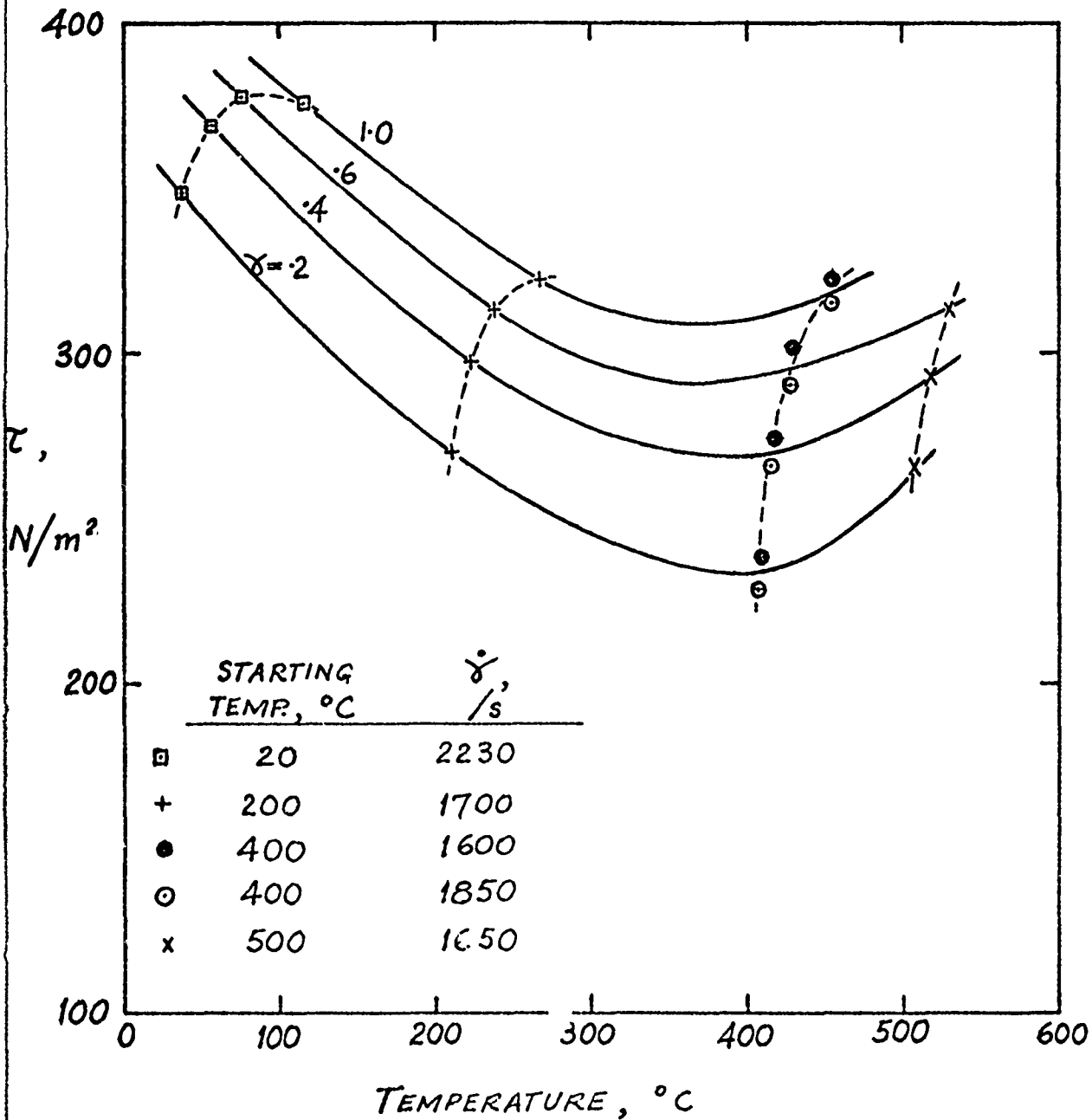

Fig. 17 Effect of total temperature on shear flow stress for different shear strains.